Electronic Energy Funnels in Cis−Trans Photoisomerization of Retinal Protonated Schiff Base†

M. Ben-Nun‡ and Todd J. Martínez*

Department of Chemistry, University of Illinois, Urbana, Illinois 61801

Received: May 20, 1998; In Final Form: August 13, 1998

The photoinduced cis−trans isomerization of all-trans retinal protonated Schiff base is studied using the full multiple spawning method. Our model allows for two classes of electronic transitions: exciton migration and quenching by coupling of the electronic and nuclear degrees of freedom. We find that quenching and exciton transfer are two temporally disjoint events and that exciton transport is highly directed. The observed selectivity in photoproducts is interpreted in terms of an electronic energy "funnel", which is attributed to the Schiff base. The limits of the concept of an electronic energy "funnel", when electron−phonon coupling is strong, are discussed and it is argued that such funnels can induce selectivity in excitation migration even when thermodynamic equilibrium among the excited electronic states is not reached.

I. Introduction

A fundamental issue in understanding the photochemistry and photophysics of extended systems is the competition between the migration of electronic excitation and the ultimate quenching of this excitation by electron-phonon coupling, i.e., nonradiative relaxation. Recent experiments and theory have brought this out in a most elegant way, for example, single-molecule spectroscopy of polyenes,[1,2] artificial dendrimeric light-harvesting systems,[3,4] excited state chemistry (both STM- and light-induced) on surfaces,[5] and fragmentation of peptide ions.[6−8] The concept of energy "funnels," which has been extensively used in other contexts,[9] provides a framework for understanding selectivity in the direction of excitation migration. However, we should recall that conventional notions of directionality induced by funnels are rooted in the assumption that the electronic degrees of freedom are in thermodynamic equilibrium. This is only clearly true when the electronic quenching rate is much slower than the rate of exciton migration. In many cases, especially in the gas phase, photochemical processes spend very little time in the electronically excited state manifold and the resulting chemistry largely occurs *after* quenching to the ground electronic state. If this ordering of time scales remains correct in the condensed phase (and/or in very large molecules), one must question the applicability of equilibrium assumptions.

An example of particular interest to us, and part of the motivation for the present study, is the case of artificial dendrimeric antenna systems.[3,4] The so-called "star dendrimers" are constructed with many concentric generations of absorbing units built around a central trap. The increasing number of absorbers in each generation leads to the desired enhanced collection efficiency, but also to an undesirable geometric bias directing electronic excitation to the periphery of the dendrimer. It has been suggested that an electronic energy funnel may be used to counteract this bias, for example by increasing the electronic excitation energy for generations closest to the dendrimer periphery. In light of the above comments, the success of this remedy appears to depend on equilibration within the excited state manifold before quenching. This quenching may be either radiative or nonradiative, but the latter is of the greatest concern since radiative lifetimes are usually very long. Of course, quenching prior to reaching the trap implies that the absorbed photon has been wasted and will be converted to heat, which may ultimately lead to decomposition of the molecule. These concerns will become more pronounced as one attempts to increase collection efficiency by increasing the number of generations in the dendrimer. This approach will lengthen the time required to reach the central trap, increasing the probability of quenching.

In this paper, we ask whether the equilibrium assumption is really necessary to observe directed excitation transport given an electronic funnel. It is important to note that we do not use the word funnel to refer to the upper/lower cone of a conical intersection, as it is sometimes used in the photochemical literature.[10,11] It is very likely that such intersections are involved in the photoisomerization process, but we speak of funnels in a less restrictive sense, referring to an energetic bias on the excited state potential energy surfaces. Our particular model is the photoinduced cis−trans isomerization of all-trans retinal protonated Schiff base (RPSB). This model is characterized by fast quenching (<500 fs), virtually guaranteeing that equilibrium among the various excited electronic states cannot be achieved before electronic quenching occurs.

RPSB is of general interest as the chromophore in the rhodopsin family of proteins, which forms a paradigm for understanding the biological mechanism of converting light into mechanical energy. Indeed, the protein systems have been the object of much experimental scrutiny,[12−16] including bacteriorhodopsin (bR) where the all-trans conformer of RPSB represents the initial state. Somewhat less attention has been paid to the dynamics of chromophore isomerization outside the protein, e.g., in solution.[17−21] The work that has been done presents several puzzles. First, the isomerization quantum yield generally exceeds 50% (64% in bR) in the protein systems, but rarely exceeds 20% in solution. The fluorescence quantum yield is low in both solution and protein environments. However,

† Dedicated to Raphael D. Levine on the occasion of his 60th birthday.

‡ E-mail: mbennun@spawn.scs.uiuc.edu.

* Corresponding author. E-mail: tjm@spawn.scs.uiuc.edu. Phone: (217) 356-9673. Fax: (217) 244-3186.

10.1021/jp9823289 CCC: $15.00
Published on Web 10/30/1998

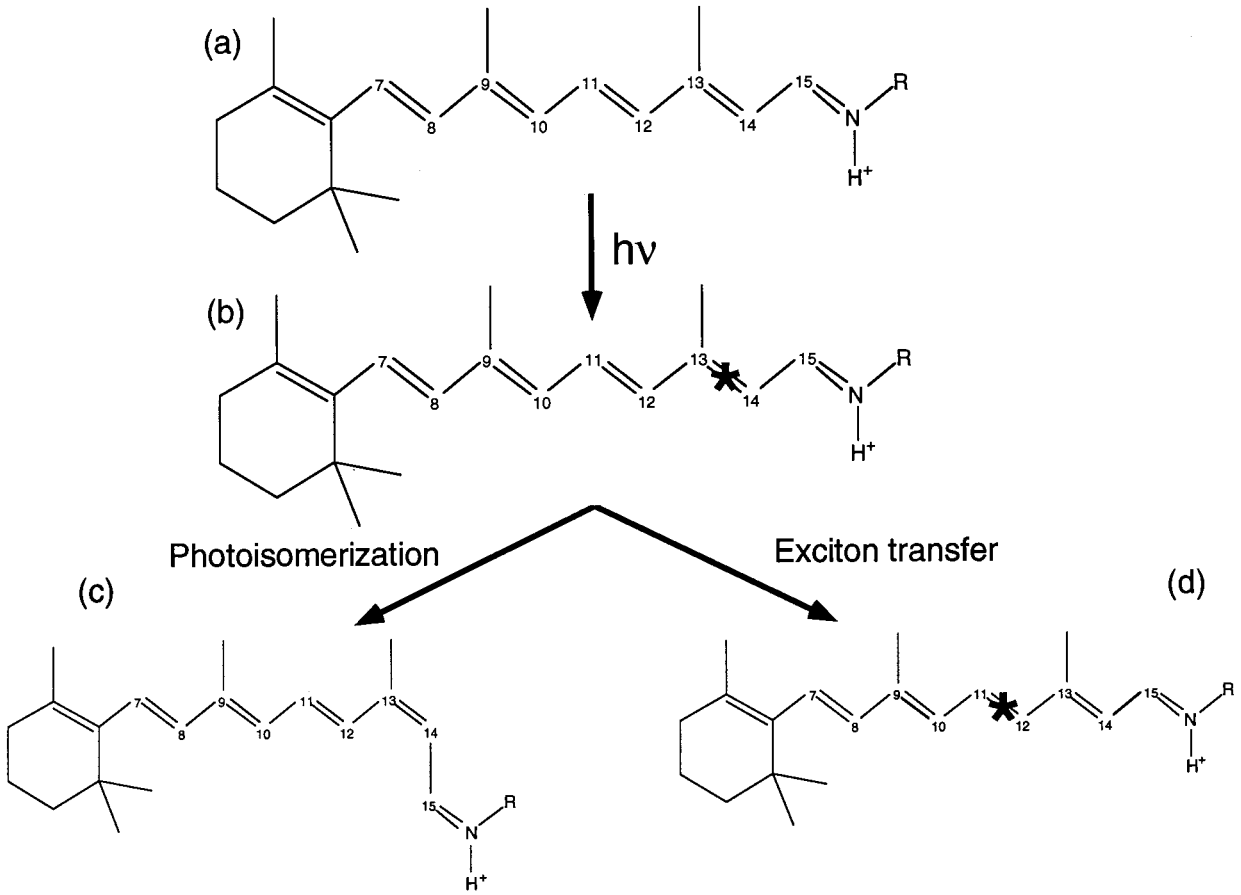

Figure 1. Schematic drawing of (a) an all-trans RPSB, (b) of a localized electronic excitation, and of the two types of non-adiabatic processes (and products thereof) considered in the model: (c) photoisomerization and (d) exciton transfer. The asterisk denotes the position of the excitation and R denotes an amine side group, taken to be lysine in our model. For clarity hydrogen atoms are not shown. In our model, the excitation may be localized on each of the five double bonds (C_7═C_8, C_9═C_{10}, C_{11}═C_{12}, C_{13}═C_{14}, C_{15}═N), it may hop between bonds [(b)→(d)] or remain on the same bond and photoisomerize [(b)→(c)]. The two scenarios depicted in this figure correspond to an all-trans → 13-cis [(a)→(c)], or all-trans → 11-cis [(a) → (d)], pathway. In this paper we use a diabatic representation and therefore the labeling of electronic states does not necessarily coincide with the geometry of the molecule. Hence, both (b) and (c) are labeled 13-cis and the only difference between them is that (c) is at the equilibrium geometry of the 13-cis state whereas the potential energy of (b) is high (see also Figure 2). Note, that in principle our model allows for any number of non-adiabatic processes (and combination thereof), and therefore an exciton transfer photoproduct, for example (d), may photoisomerize and/or transfer the excitation.

the time scales for isomerization are quite different, with reports ranging from 200 fs to 2 ps in proteins[13] or solution,[21] respectively. Furthermore, the photoproducts in protein environments can be quite different from those in solution. In bR, isomerization of all-trans RPSB about the C_{13}═C_{14} double bond predominates, while in solution one observes primarily C_{11}═C_{12} isomerization. Therefore the ordered protein environment plays an important role in altering the course of the photochemistry.

Since one observes isomerization almost exclusively about a specific C═C bond, both in protein and solution, it might be useful to view RPSB as a collection of coupled absorbers. This unconventional picture emphasizes the local character of the double bonds rather than the extended conjugation of the molecule, and may essentially be considered as a valence-bond (VB) picture of the electronic structure, in contrast to the more often used molecular orbital (MO) picture. The VB picture allows for a natural interpretation of dynamics in terms of interplay between exciton transfer and nuclear motion; however, many electronic states must be considered. That is, even when there is only one important delocalized excited electronic state, the VB picture describes it as a superposition of many localized states.

Because of the protonated Schiff base on one end of the molecule, each of these local absorbers will have a slightly different excitation energy. In particular, the positive charge at the Schiff base leads one to expect an increasing red shift (relative to the C═C absorption in a C-only polyene of the same length) progressing from the ionone ring to the Schiff base (see Figure 1a). In the context of this local picture, there are two possible explanations for the different photoproducts in bR and in solution. The first possibility is that the protein alters the relative oscillator strengths of the C═C bonds. Provided excitation migration is slow, this leads straightforwardly to selectivity in isomerization. A second possibility stems from the obvious observation that the protein sterically hinders isomerization about many of the candidate double bonds. Thus, one could imagine that absorption at deselected bonds would cause an unsuccessful attempt at isomerization and conversion of the photon energy to heat or possibly fluorescence. This cannot be the whole story because the photoisomerization quantum yield is enhanced in the protein while the fluorescence quantum yield is unaffected. However, if exciton migration occurs, one can imagine that the excitation might walk along the double bonds, attempting isomerization at each until successful. Each unsuccessful attempt will carry some probability of electronic quenching. Considerations of efficiency then dictate that excitation migration is not a random walk, but rather directed toward the selected bond, thereby minimizing

the quenching probability. We suggest that such directionality may be imposed by the energetic funnel induced by the Schiff base, in spite of the strong nonequilibrium nature of the photoisomerization process.

Both of the competing processes under consideration, exciton migration and quenching, involve electronic transitions. We have recently developed the full multiple spawning (FMS) method[22−25] that can efficiently and accurately treat such nonadiabatic dynamics, and we employ this approach here. The accuracy of the method has been demonstrated by explicit comparison to numerical solution of the Schrödinger equation for a multidimensional, strongly coupled, anharmonic model problem.[25] Quantitative agreement was obtained for the quantities compared, for times up to a picosecond. Our recent study of the photodynamics of bacteriorhodopsin,[26] where all degrees of freedom (>11 000) were treated quantum mechanically, attests to the efficiency and applicability to large systems.

We begin with a short discussion of the FMS method, followed by a discussion of the potential energy surfaces used for RPSB. Results of the simulations are then presented, and we explain how an electronic energy bias can direct photochemistry even on the sub-picosecond time scale. We conclude by relating our results to experiments on RPSB in solution and protein environments and to the question of electronic energy funnels and their influence on selectivity for ultrafast processes.

II. Theory

The FMS method has previously been discussed in detail (see refs 24 and 25) and we review it only briefly in what follows. The method uses an adaptive, time-dependent basis for the wave function. They key idea behind the method is to expand the size of the basis during non-adiabatic events, using the available information to predict the regions in phase space where population will be created. This dynamical expansion of the number of basis functions is accomplished via a spawning procedure that keeps the basis size manageable while ensuring that it provides a reasonable approximation to the exact wave function. Because classical mechanics serves as a guide for basis set selection and propagation the computational effort remains classical-like, yet quantum mechanical effects are included.

Consider the general multielectronic state Hamiltonian operator

$$\hat{H} = \sum_I |I\rangle \hat{H}_{II} \langle I| + \sum_{I \neq I'} |I\rangle \hat{H}_{II'} \langle I'| \qquad (2.1)$$

where the orthonormal electronic states I are donated in bracket notation and the operators $\hat{H}_{II}$ and $\hat{H}_{II'}$ act only on the nuclear degrees of freedom. (Atomic units are used in this paper, i.e., $\hbar = m_e = 1$.) The FMS method uses a Born−Oppenheimer wave function ansatz of the form

$$\Psi = \sum_I C_I(t) \chi_I(\mathbf{R};t) |I\rangle \qquad (2.2)$$

that can be applied for any number of electronic states and nuclear degrees of freedom. In eq 2.2 the total wave function Ψ is expressed as a weighted sum over electronic states, where each component in the sum is a product of an electronic wave function and a multidimensional time-dependent nuclear wave function. (Throughout this paper bold letters are used to denote vectors and matrices.) Note that since each electronic state has its own nuclear wave function, one has direct access to dynamical quantities on each electronic state. The time-dependent wave function for the Ith electronic state is represented as a linear combination of multidimensional Gaussian basis functions[27] with time-dependent amplitudes

$$\chi_I(\mathbf{R};t) = \sum_j d_{I,j}(t) \chi_j^I(\mathbf{R};\bar{\mathbf{R}}_j^I(t),\bar{\mathbf{P}}_j^I(t),\bar{\gamma}_j^I(t),\alpha_j^I) \qquad (2.3)$$

Here the indices I and j label the jth nuclear basis function on electronic state I, and all the time dependencies of the basis functions are explicitly denoted. For multidimensional problems, it is most convenient to use a Cartesian coordinate system and construct each of the multidimensional Gaussian basis functions in eq 2.3 as a product of $3N$ one-dimensional Gaussian functions

$$\chi_j^I(\mathbf{R};\bar{\mathbf{R}}_j^I(t),\bar{\mathbf{P}}_j^I(t),\bar{\gamma}_j^I(t),\alpha_j^I) = \exp(i\bar{\gamma}_j^I(t)) \prod_{\rho=1}^{3N} \tilde{\chi}_{\rho_j}^I(R_\rho;\bar{R}_{\rho j}^I(t),\bar{P}_{\rho j}^I(t),\alpha_{\rho j}^I) \qquad (2.4)$$

$$\tilde{\chi}_{\rho_j}^I(R_\rho;\bar{R}_{\rho j}^I(t),\bar{P}_{\rho j}^I(t),\alpha_{\rho j}^I) = \left(\frac{2\alpha_{\rho j}^I}{\pi}\right)^{1/4} \exp\{-\alpha_{\rho j}^I[R_\rho - \bar{R}_{\rho j}^I(t)]^2 + i\bar{P}_{\rho j}^I(t)[R_\rho - \bar{R}_{\rho j}^I(t)]\} \qquad (2.5)$$

The index ρ, $\rho = 1, 2 \ldots, 3N$ enumerates the $3N$ Cartesian coordinates for a system with N atoms and each Gaussian has a time-independent width $\alpha_{\rho j}^I$. In the special case of harmonic potentials, the natural choice for this width is related to mass and frequency.[27,28] However, for general potentials, the choice is not clear and the width is best viewed as a parameter chosen heuristically; it has been previously found that for suitable ranges of parameter values, the results are independent of its specific value. The time evolution of the phase space parameters in each Gaussian is described by Hamilton's equation of motion. Hence, each Gaussian state is centered along a classical trajectory whose time evolution is determined by the potential of the Ith electronic state

$$\dot{\bar{R}}_{\rho j}^I(t) = \dot{\bar{P}}_{\rho j}^I(t)/M_\rho; \quad \bar{P}_{\rho j}^I(t) = -\partial V_I(\mathbf{R})/\partial R_{\rho j}|\bar{R}_{\rho_j}^I(t) \qquad (2.6)$$

The time evolution of the nuclear phase $\bar{\gamma}_j^I(t)$ is described by

$$\dot{\bar{\gamma}}_j^I(t) = \sum_{\rho=1}^{3N} \frac{1}{2M_\rho}[(\bar{P}_{\rho j}^I(t))^2 - 2\alpha_{\rho j}^I] - V_I(\bar{R}_j^I(t)) \qquad (2.7)$$

which involves the classical Lagrangian as well as a contribution from the width of the Gaussian state. In eqs 2.6 and 2.7 the over-dot denotes a time derivative, M_ρ is the mass of the ρth atom, and $V_I(\mathbf{R})$ is the potential energy for state I. Note that a single nuclear phase factor is associated with each multidimensional Gaussian [cf. eq (2.4)].

The time-dependent coefficients $D_j^I(t) = C_I(t)d_{I,j}(t)$ are the probability amplitudes for being in nuclear basis state j on electronic state I at time t. Given the orthonormality of the electronic states, a set of coupled equations of motion for these coefficients is obtained by substituting the wave function ansatz of eqs 2.2−2.5 into the time-dependent Schrödinger equation, or equivalently by using the time-dependent variational principle.[29−31] The resulting equation of motion is

$$\dot{\mathbf{D}}^I = -i(\mathbf{S}_I)^{-1}\{[\mathbf{H}_{II} - i\dot{\mathbf{S}}_I]\mathbf{D}^I + \sum_{I \neq I'} \mathbf{H}_{II'}\mathbf{D}_{I'}\} \qquad (2.8)$$

where $\mathbf{S}_I$ is the time-dependent nuclear overlap matrix of the

Gaussian basis functions on electronic surface I, $\mathbf{H}_{II'}$ is the subblock of the Hamiltonian matrix describing the interaction between basis functions on electronic state I and I' (or between two basis functions on the same electronic state, i.e., $I = I'$), and $\dot{\mathbf{S}}_I$ is the matrix representation of the right-acting time derivative operator.

The set of coupled equations of motion for the electronic and nuclear degrees of freedom [eqs 2.8 and 2.6−2.7 respectively] are the working equations for the FMS method. Having detailed them we now discuss the selection of basis functions representing population created after a nonadiabatic event. We refer to the dynamical expansion of the basis set as spawning. The technique of spawning is one of the most important features of the method governing both its numerical convergence and computational feasibility. Basis functions are added to the basis set, i.e., spawned, only during nonadiabatic events and hence we must first define a "nonadiabatic event". We define an effective nonadiabatic coupling for each basis function in the diabatic representation as

$$\mathbf{H}_{II'}^{\text{eff}} = \left| \frac{\langle I|\hat{H}_{II'}|I'\rangle}{V_I(\mathbf{R}) - V_{I'}(\mathbf{R})} \right| \tag{2.9}$$

When the magnitude of this effective coupling for a given basis function exceeds a predetermined threshold, this basis function is considered to be in a non-adiabatic region. At this time, basis functions which will represent the non-adiabatic population transfer must be created, i.e., spawned, on the coupled electronic state (I'). For problems of chemical interest, the regions of effective nonadiabatic coupling are typically spatially localized.[10,32] Therefore, by introducing the concept of a nonadiabatic event, unnecessary spawning attempts are avoided when the interstate coupling is negligible.

Once a basis function has entered a nonadiabatic region, it is propagated until the effective coupling decreases below the spawning threshold in order to determine the "crossing time:" the time during which the effective nonadiabatic coupling exceeds the spawning threshold. The crossing time is divided into N_s equal intervals and within each of these intervals a basis function will be spawned with zero population and with maximal overlap with its parent. (Thus, N_s is the number of spawned basis functions per traversal of the nonadiabatic region.) The classical energy of the spawned basis functions is required to be the same as that of its parent and therefore its momentum needs to be adjusted. Herman has demonstrated[33] that the best possible momentum adjustment (in the near-classical limit) is along the nonadiabatic coupling vector (this adjustment was previously used by Tully[34] on physical grounds). Once the position and momentum of the newly spawned basis functions are known, they and the parent function are propagated backward in time to the beginning of the nonadiabatic event. The actual forward propagation continues at this point, including the solution of the trajectory amplitudes for the newly spawned basis functions. The procedure that we use allows also for back spawning, i.e., a newly populated electronic state is allowed to transfer population back to the other electronic state. Furthermore, attempts to spawn basis functions that are redundant with other (occupied or unoccupied) basis functions on the same electronic state are rejected. By doing so we avoid the wasteful spawning of basis functions which, in any case, will be removed when the nuclear overlap matrix [**S** in eq 2.8] is inverted by a singular-value-decomposition procedure.[35]

Many technical details, such as the specific choice of the various parameters that govern the numerical convergence of the method, as well as the initial values of the electronic and nuclear parameters are discussed in section III.B.

III. Model and Results

A. Potential Energy Surfaces. As discussed in the introduction, our model takes the initial electronic state to be locally excited and it allows for two types of nonadiabatic processes: exciton transfer and quenching (the possible formation of diradical electronic states, i.e., solitons, is ignored.) The assumption of local excitation is for convenience of interpretation—a delocalized initial state can be viewed as a coherent superposition of the locally excited states. Six potential energy surfaces (PESs), describing electronic states with differing equilibrium conformations (all-trans, 15-cis, 13-cis, 11-cis, 9-cis, and 7-cis, with atom numbering as in Figure 1) are used to model these non-adiabatic processes. We first describe the construction of the diabatic potentials and then proceed to discuss their couplings.

The all-trans equilibrium structure is based on a model by Santarsiero and James.[36] A modified version[37,38] of the charmm19 force field and parameters[39] was used as a starting point for the six PESs. The all-trans and each of the other five electronic state potentials differ in two degrees of freedom: the stretching and torsion of one (C_{15}═N, C_{13}═C_{14}, C_{11}═C_{12}, C_9═C_{10}, C_7═C_8) of the double bonds. By allowing the electronic states to differ in more than one degree of freedom, we account for the possibility of true crossings, i.e., conical intersections, between the states.[40]

On each of the six electronic states, the dominant contribution to the functional form of the torsion around a given double bond j is given by

$$E_j^I = k_j^I[1 + \cos(\phi_j + \delta_j^I)] \tag{3.1}$$

Here, I is an electronic state index, $2k_j^I$ is the endothermicity for rotation around bond j on electronic state I, ϕ_j is the torsion angle, and δ_j^I is a phase factor. The all-trans electronic state potential has a single global minimum with all torsional angles in a trans conformation, i.e., $\delta_j^{\text{all-trans}} = 0$. Each of the other five electronic states has an equilibrium geometry with one *cis* double bond and all other double bonds in a trans conformation. Hence, the 13-cis state, for example, is obtained by setting $\delta_{C_{13}=C_{14}}^{13-\text{cis}}$ to π, and similarly for other states. Note that we label the electronic states by the nuclear configuration in their global minimum, and this labeling does not necessarily coincide with the geometry of the molecule. For example, on the all-trans state, one (or more) of the dihedral angle(s) could be in a cis conformation, i.e., $\phi_j \approx 0°$. In this case the potential energy would be high (see Figure 2a below), but the electronic state would still be labeled all-trans. A similar situation can occur on any of the other electronic states. Thus, the electronic state labeling coincides with the geometry of the molecule only when the latter is at or near equilibrium, i.e., low potential energy.

Transient spectroscopy experiments of El-Sayed et al.[21] on the excited-state dynamics of RPSB in solution suggest a barrier of $\approx$600 cm^{-1} in the excited state (which results from intramolecular electronic factors and not from the solvent viscosity). Hence, we augment the functional form of eq 3.1 with a Gaussian term describing this barrier:

$$E_j^I = k_j^I[1 + \cos(\phi_j + \delta_j^I)] + A \exp[-b(\phi_j - (\phi_0 - \delta_j^I))^2] \tag{3.2}$$

Given a certain value for k_j^I (see below), the parameters A, b,

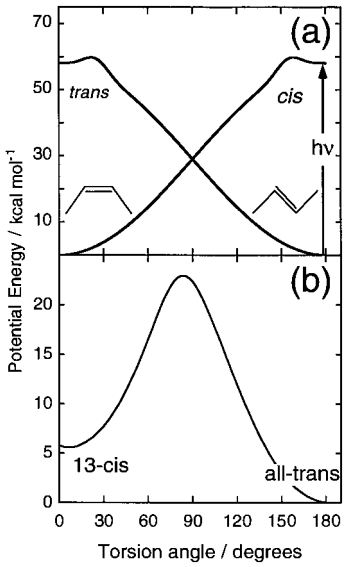

Figure 2. (a) Functional form of the all-trans and 13-cis PESs, assumed in the computation, as a function of the C_{13}═C_{14} torsion angle. (The functional form of the dihedral energy, eq 3.2, is the same for all five dihedral angles.) The arrow indicates the electronic excitation. In the diabatic representation (adopted in this paper), the labeling of the diabatic electronic states coincides with the geometry of the molecule only when the latter is at (or about) its equilibrium geometry. Hence, as the dihedral angle changes from 180° to 0° and one moves diabatically on the trans (cis) curve the electronic state labeling remains trans (cis) but the geometry varies from trans, right inset, to cis left inset. (b) Minimum energy path along the ground adiabatic state for torsion around the C_{13}═C_{14} bond.

and ϕ_0 are adjusted so that eq 3.2 reproduces a barrier of 600 cm^{-1} for torsion about each of the four dihedral angles involving C═C bonds and 1000 cm^{-1} for the torsion about the C_{15}═N bond. On all six electronic states, the same force constant, k_j^I = 29 kcal/mol, is assumed for all four dihedral angles that involve a torsion around a C═C bond. This value is very similar to the one used previously by Humphrey et al.[37] The resulting local vertical excitation energies for all-trans → 13-cis and all-trans → 11-cis are 447 and 440 nm, respectively. These values are comparable to the experimentally observed absorption maximum of RPSB in various solvents, e.g., methanol, acetonitrile, and hexane. The magnitude of $k^I_{C_{15}=N}$ for the torsion around the C_{15}═N bond is not adjusted, and we use the value (14.2 kcal/mol) suggested by Humphrey et al.[37] Figure 2a illustrates the energy dependence of the ground all-trans state and the 13-cis state on the C_{13}═C_{14} dihedral angle. The *functional form* of the dihedral energy for all the double bonds on all the diabatic states is the same. Furthermore, for the four C═C dihedral angles the plots are identical and their scale (yet again not form) is different only for the torsion about the C_{15}═N bond. (However, we wish to emphasize that the dependence of the *total* energy on the dihedral angle is naturally different for the five relevant dihedral angles, because the total energy is not restricted to dihedral terms.)

The diabatic electronic state potentials differ in one more degree of freedom: the C═C stretching force constant and equilibrium distance of one of the relevant five double bonds. Because of the delocalization of the positive charge near the Schiff base, the C═C bond orders will decrease progressing from the ionone ring to the Schiff base. This is observed in the X-ray structure[36] as a decrease in the C═C bond length as one recedes from the Schiff base end of the molecule. Excitation of the molecule in an all-trans geometry from the all-trans electronic state to any of the five other states corresponds to the promotion of a π electron to a π^* orbital. Thus, it is clear that the magnitude of one of the stretching force constants on each of the excited states should be lowered. In order to determine by how much we should lower each force constant, we first determine the bond orders on the all-trans state. To a zeroth approximation, we assume that the fractional decrease in bond order on each of the excited states (in the all-trans geometry) is the same. We have evaluated the ground state bond orders, n_j, for the five relevant bonds using the X-ray structure and the Pauling bond-length−bond-order relationship,[41] with a value of 1.5 Å for the bond length of a C−C single bond. The results, together with the ground state equilibrium bond distances, are listed in Table 1. The bond order decreases from 1.7 to 1.5 as one moves along the retinal backbone, i.e., from C_7═C_8 to C_{13}═C_{14}. Given these bond orders we define a "typical" stretching force constant for unit bond order by dividing the ground state force constant of the C_{13}═C_{14} bond by its bond order. This results in a "typical" force constant for a C−C stretch of 380 kcal/mol Å^2, and this is the value that we use for the C_{13}═C_{14} stretch on the 13-cis state (all the other stretching force constant are kept at their ground state value). The stretching force constants ($k_s^{I,j}$) for the C_7═C_8, C_9═C_{10}, and C_{11}═C_{12} bonds on the 7-cis, 9-cis, and 11-cis states, respectively, are determined relative to this force constant using the relation: $k_s^{I,j} = k_s^0(n_j/n_{C_{13}=C_{14}})$ and k_s^0 = 380 kcal/mol Å^2. Note that this equation correctly reproduces the linear scaling of stretching force constants with bond order[42] and that it also retains the trend in bond order that is observed on the ground state. For simplicity, we have set the equilibrium bond length of the (relevant) C═C bond on each of the four excited states to be 1.5 Å. Table 1 summarizes the excited state stretching force constants obtained by this procedure. The overall variation is ∼10%. Table 1 also lists the ground state bond order and length for the C_{15}═N bond and $k_s^{15-cis,C_{15}=N}$ (C_{15}═N stretching force constant on the 15-cis state). For this bond, the Pauling relationship was again used to determine the ground state bond order with the C−N bond length for unit bond order being 1.475 Å. The "typical" C−N force constant for unit bond order was determined by dividing the ground state force constant by the ground state bond order.

TABLE 1: Ground State Equilibrium Distances (r_{eq}) and Bond Orders, and Excited State Stretching Force Constants ($k_s^{I,j}$)

	ground state		excited states	
bond	r_{eq}(Å)	bond order	electronic state	$k_s^{I,j}$ (kcal mol^{-1} Å^{-2})
C_{15}═N	1.324	1.5	15-cis	320
C_{13}═C_{14}	1.368	1.53	13-cis	380
C_{11}═C_{12}	1.357	1.59	11-cis	394
C_9═C_{10}	1.354	1.61	9-cis	400
C_7═C_8	1.336	1.7	7-cis	422

The above-described excited state potentials are deficient in that at the minimum of each of the five excited cis states, the relevant internuclear equilibrium distance and stretching force constant is not the same as that of the all-trans state. This is a consequence of the diabatic representation assumed in this paper. Within this representation the only way to correct this unphysical behavior would be to allow the relevant stretching force constant and equilibrium distance on each of the five excited states to be a function of its torsion angle. This would affect the vibrational distributions of the photoproducts, but will have negligible effect on the short-time dynamics which interests us in this paper.

Our model requires two types of nonadiabatic coupling terms: an intra-bond coupling term that describes quenching,

(i.e., population transfer between an excited state and the all-trans state) and an interbond term that describes exciton transfer, i.e., population transfer between two excited states. We assume that the coupling between the all-trans state and each of the five excited states is constant and the same for all excited states. Its value has been set to 10 kcal/mol, leading to a C=C isomerization barrier of ≈24 kcal/mol. An exponential form is assumed for the interbond coupling so that the exciton is expected to prefer to hop between two adjacent bonds. The resulting 6 × 6 Hamiltonian matrix is

$$\hat{H} = \begin{bmatrix} H_{(\text{all-trans})} & V & V & V & V & V \\ V & H_{(15\text{-cis})} & Ve^{-c} & Ve^{-2c} & Ve^{-3c} & Ve^{-4c} \\ V & Ve^{-c} & H_{(13\text{-cis})} & Ve^{-c} & Ve^{-2c} & Ve^{-3c} \\ V & Ve^{-2c} & Ve^{-c} & H_{(11\text{-cis})} & Ve^{-c} & Ve^{-2c} \\ V & Ve^{-3c} & Ve^{-2c} & Ve^{-c} & H_{(9\text{-cis})} & Ve^{-c} \\ V & Ve^{-4c} & Ve^{-3c} & Ve^{-2c} & Ve^{-c} & H_{(7\text{-cis})} \end{bmatrix} \tag{3.3}$$

The parameters used in the simulations, $c = 1.5$ and $V = 10$ kcal/mol, result in a nearest-bond exciton coupling of 2.3 kcal/mol and a next-nearest coupling that is practically zero. We do not make any distinction between C=C and C=N bonds in our model. This leads to the possibility of excitation migration to, and subsequent isomerization about, the C=N bond which is not observed experimentally. A more accurate model would use different exciton couplings. However, since our primary goal here is understanding the phenomenology of electronic funnels in photochemistry, a single coupling strength will suffice.

A diabatic representation has been used in all the computations discussed in section III.C. It is important to verify that the model also results in a reasonable isomerization pathway in the adiabatic representation. In Figure 2b, we show the reaction path for isomerization about the C_{13}=C_{14} bond on the adiabatic ground state. This figure shows that the model results in a smooth isomerization pathway in the adiabatic as well as diabatic representation.

B. Technical Details. The FMS method is derived from a variational principle and therefore it must converge to the exact quantum mechanical result, provided enough basis functions are used. In the simulations performed in this paper, all 68 atoms of RPSB are explicitly included. The multidimensional nuclear wave function [eq 2.4] is therefore written as a product of 3 × 68 = 204 one-dimensional Gaussian functions. For such a large system, ensuring numerical convergence with respect to all the parameters that define the time dependent basis set, and govern its size, is not a simple matter. Therefore, we have performed extensive tests to ensure convergence, as detailed below.

The same width parameter $\alpha_{\rho j}^{I}$ was used for all the coordinates on all six surfaces and its value was set to 10 bohr^{-2}. This value is consistent with typical values obtained for C−C and C−H bonds in the harmonic approximation. Furthermore, short-time test simulations showed that the branching ratio is insensitive to the width parameter for choices in the range 8-14 bohr^{-2}. Test simulations were also used to determine the magnitude of the effective coupling that triggers spawning [eq 2.9]. By running sample trajectories and examining the magnitude of the effective nonadiabatic coupling (as a function of time), we have verified that a threshold value of 0.9 is appropriate. This value does not miss any of the nonadiabatic events, which are typically indicated by "spikes" in the effective coupling.[43] The number of spawned basis functions per traversal of the nonadiabatic region N_s was set to three. Short-time (≈100 fs) test simulations verified that the results are very similar (branching ratios within 5%) for $N_s = 3$ and $N_s = 5$. In a typical propagation, these parameters lead to a total of about 250 spawned basis functions.

Two local electronic excitations were modeled: all-trans → 13-cis and all-trans → 11-*cis*. Initially only the excited state, either 13-cis or 11-cis, is populated and the initial state is modeled as a stationary state using a linear combination of three coherent states. Each of these coherent states is parameterized by ten classical trajectories. The initial conditions for the basis functions were selected using the following procedure. RPSB was equilibrated on the all-trans electronic state for 20 ps and three uncorrelated (1 ps apart) sets of 10 correlated configurations (∼0.5 fs apart) were selected as initial structures for the basis functions. In each of the three coherent states the initial amplitude of each (of the 10) basis functions is set to 0.1 and the 10 basis functions are propagated simultaneously. The results that we report in the next section are incoherently averaged over three such sets of runs. The variation in the final electronic state populations for the averaged runs is typically less than 5%. The simulations were carried out in vacuum at 300 K, with a uniform dielectric constant of 1 and a 14 Å cutoff for Coulomb forces. Neither solvent molecules nor a counterion are present in our model. This is expected to significantly decrease the photoisomerization time scale compared to experiments performed in solution.

A split-operator procedure[44] was used to propagate the set of coupled nuclear and electronic equations of motion [eqs 2.6, 2.7, and 2.8, respectively] in the diabatic representation. This approximation avoids the need to evaluate the time derivative of the nuclear overlap matrix [$\dot{\mathbf{S}}$ in eq 2.8] and the diagonal elements of the Hamiltonian [$\mathbf{H}_{II}$ in eq 2.8]. Since the six diabatic surfaces are coupled by constant potential energy coupling terms [see eq 3.3], the off-diagonal matrix elements of the Hamiltonian [$\mathbf{H}_{II'}$ in eq 2.8] can be evaluated analytically. A time step of 1 fs was used for the propagation and it was lowered to 0.2 fs whenever a basis function was in a spawning mode.

C. Results. We will focus most, yet not all, of our discussion on branching ratios, paying special attention to the details of the population transfer as a function of time, and to the coupling between the electronic and nuclear motions. As will be argued below, the strong coupling between these motions governs the time scale of exciton hopping (population transfer in the manifold of adiabatic excited states) and the onset of quenching (population transfer back to the adiabatic ground electronic state). Because the analysis of the dynamics on six coupled electronic states is quite complicated, we wish to stress again that the labeling of diabatic electronic states (all-trans, 15-cis, etc.) does not necessarily coincide with the geometry of the molecule, i.e., with the magnitude of the five relevant dihedral angles. When it does the RPSB is at (or close to) equilibrium whereas if it does not the potential energy is high.

The two sets of computations begin with basis functions on either the 13-cis or 11-cis state, in the all-trans nuclear geometry. In Figure 3, parts a and b, we show the reaction probability as a function of time for these two local excitations. This Figure demonstrates many important points that are crucial for the analysis of the two nonadiabatic processes in question: exciton hopping and quenching back to the initial all-trans electronic

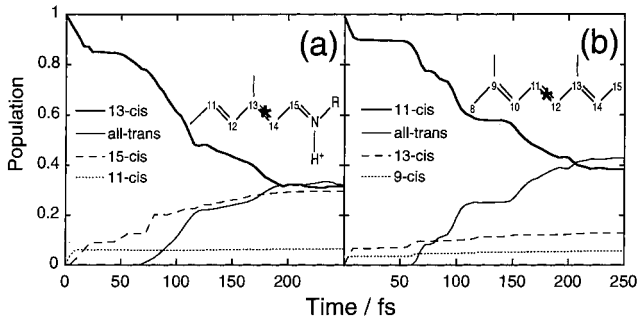

Figure 3. (a) Population on the initially excited 13-cis electronic state (heavy full line) and on the 15-cis, 11-cis, and all-trans states (dashed, dotted, and full thin line, respectively) as a function of time in femtoseconds. (The results are averaged over 3 runs and in each run 10 basis functions are used to represent the initial wave function.) The inset indicates the retinal backbone and initial excitation. Note that the time scale for exciton transfer to the 15-cis state is much longer than to the 11-cis state and that exciton transfer precedes quenching back to the all-trans state. (b) Same as (a) but for an initial excitation of the 11-cis electronic state (see inset). Full heavy line: 11-cis state. Dashed line: 13-cis state. Dotted line: 9-cis state. Full thin line: all-trans state. Unlike part a, here the time scale for exciton transfer to the 13- and 9-cis states is similar but the amount that is transferred is not: there is a clear bias toward the 13-cis state. The time ordering of the two non-adiabatic processes is as in part a: exciton transfer precedes quenching to the ground state.

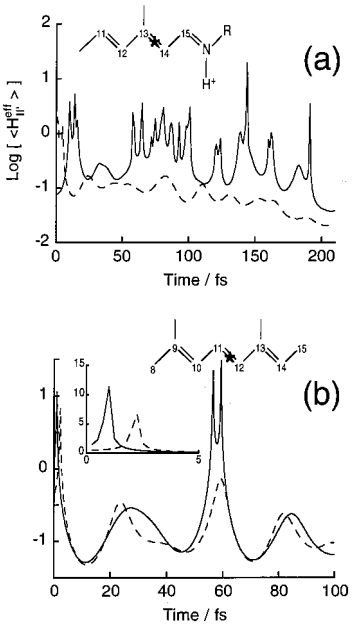

Figure 4. (a) Logarithm of the magnitude of the average effective nonadiabatic coupling (eq 2.9) as a function of time in femtoseconds. The initial excitation is to the 13-cis state (see inset). Full and dashed lines denote the coupling to the 15- and 11-cis states, respectively. The coupling is evaluated for one of the three runs using the ten initially populated basis functions. In agreement with Figure 3a, the coupling to the 15-cis state is stronger and it extends over a longer time period. (b) As in part a but for an initial excitation of the 11-cis state. The inset shows the short time behavior. In agreement with Figure 3b the time scale during which the initially excited state is coupled to the 13- and 9-cis states is similar yet the magnitude of the coupling to the 13-cis state is somewhat stronger.

state. First, we see that the two processes begin at quite different points in time: exciton transfer precedes quenching. Since the crossing between the all-trans state and any of the five excited states is at a dihedral angle of 90° this result is not surprising. Quenching back to the all-trans electronic state requires a substantial motion along the relevant torsion coordinate (a particular dihedral angle, e.g., $\phi_{C_{13}=C_{14}}$ for 13-cis and $\phi_{C_{11}=C_{12}}$ for 11-cis) and hence its delayed onset. In contrast exciton transfer may (and does) occur instantaneously as it does not require any nuclear rearrangement. In fact, as will be discussed further below, exciton transfer is shut off as the nuclear motion progresses along the isomerization coordinate.

Second, we see that in both cases the local excitation results in only three photoproducts. Two are formed via exciton transfer [the exciton hops to the two nearest bonds (≡states)] followed by photoisomerization, whereas the third is a result of photoisomerization at the bond which was initially excited. Thus excitation of, for example, the $C_{11}=C_{12}$ bond results in regeneration of all-trans RPSB and the following photoproducts: 9-cis, 11-cis, and 13-cis RPSB. Note that all of the cis electronic states may lead back to the all-trans RPSB, i.e., all-trans RPSB may be formed with or without exciton transfer. However, the 9-cis and 13-cis RPSB products require exciton transfer. The yield of the two photoproducts via exciton transfer is not symmetric. There is an observed preference for photoproducts that involve isomerization about a dihedral angle closer to the Schiff base end of the RPSB. When the 11-cis state is excited (Figure 3b) the time scale for exciton transfer up and down the retinal backbone, i.e., to states 13-cis and 9-cis, is very similar. Nevertheless, more population transfer occurs in the upward direction. (The final population on the 13-cis state is 0.13, whereas on the 9-cis state it is 0.06.) This bias is more pronounced when the 13-cis state is excited (Figure 3a): the final population on the 15-cis state is 0.30, whereas on the 11-cis state it is 0.07. Furthermore, for this local excitation the time scale for exciton transfer to the 15-cis state is much longer than to the 11-cis state. Similar effects were observed in simulations (not shown) using stronger coupling [increasing c in eq 3.3] between the excited electronic states. In order to understand these results we have examined the potential energies on the various electronic states and the effective nonadiabatic coupling between electronic states as a function of time. We begin by discussing the results shown in Figure 3a, i.e., excitation of the 13-cis state.

In Figure 4a we plot the (logarithm of the) average effective non-adiabatic coupling evaluated along the trajectories of the initial basis functions, between the initially excited 13-cis electronic state and the 11- and 15-cis electronic states. The time dependence of the population transfer (Figure 3a) is expected to follow the behavior of the non-adiabatic coupling, and indeed we find that, compared to the 11-cis state, the coupling to the 15-cis state is stronger and extends over a longer time period. According to Figure 4a, the nonadiabatic coupling between the 13-cis and 11-cis states decreases to zero very quickly suggesting that this property is strongly dependent on the nuclear dynamics. Since in our model the diabatic coupling between any two electronic states is constant, i.e., it is not a function of any of the dihedral angles, see eq 3.3, the effective nonadiabatic coupling is determined only by the energy difference between the two electronic states (the denominator in eq 2.9). Hence, in order to understand the trends that we observe in Figure 3a, we must understand the time dependence of the energies on the three relevant electronic states.

The PESs of the five excited states are identical except for two torsional and two stretching modes. We find that the difference in torsional motion dominates the energy difference for this case, and hence we first restrict our attention to this coordinate. Immediately after the optical excitation, the nuclear geometry is out of equilibrium for *all* excited electronic states. In particular, the torsional angle for each of the bonds is ≈180°, while the equilibrium value for one of the bonds on each of the

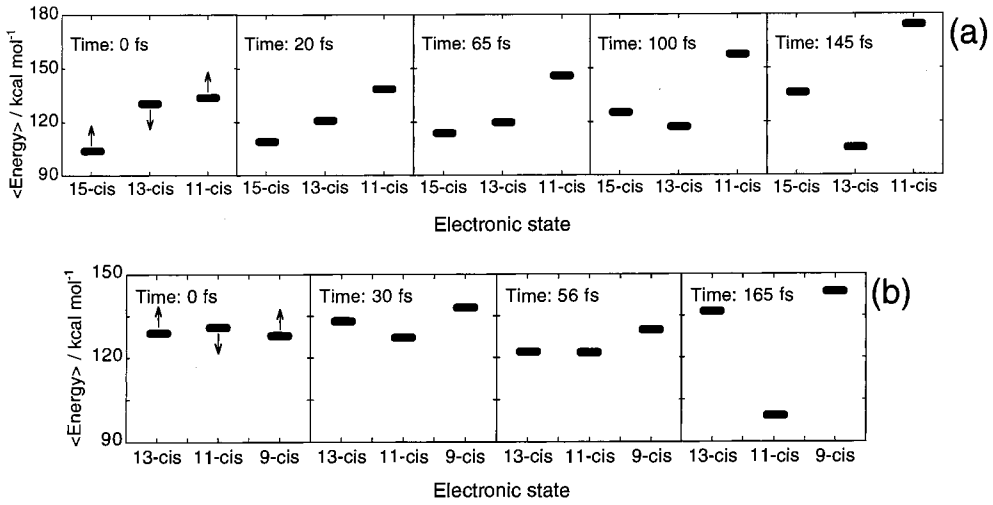

Figure 5. Snapshots of the average potential energies of the labeled electronic states for the geometry of the initially populated basis states. The initial excitation is to the 13-cis state (see inset) and the averaging is as in Figure 4. The arrows (left most panel) indicate the overall direction in which the potential energies on the different electronic states change (see text for more details about the reason for the directions shown). As discussed in Section III.C the time duration and magnitude of the effective nonadiabatic coupling (and hence of population transfer) is determined by the duration and extent of resonance between the initially excited state, 13-cis, and the exciton transfer states: 15- and 11-cis. The initial values of the energies, combined with the direction in which they move, explains the time dependence of the effective nonadiabatic coupling (Figure 4a) and of the population transfer (Figure 3a). (b) As in part a but for initial excitation of the 11-cis state. Note that the energy scale in this panel is different (smaller) than in part a and the differences between the two photoproduct states (13- and 9-cis) are not as pronounced. As in part a, the overall direction in which the potential energies on the different electronic states move is indicated by the arrows (leftmost panel). Because the energy scale in this panel is smaller one can see the oscillations (due to vibrations, bendings and librations) which are superimposed on this overall direction. The time scale during which the initially excited state is in resonance with the 13- and 9-cis states is similar but within this time scale the energies on the 11- and 13-cis states are somewhat closer than those on the 11- and 9-cis states. This is the reason for the bias in population transfer and effective coupling of the 11-cis and 13-cis states (Figures 3b and 4b, respectively). See text for more details.

excited states is ≈0°. If the 13-cis state is excited then the torsion angle about the C_{13}═C_{14} bond, $\phi_{C_{13}=C_{14}}(t)$, will begin to vary in time until it approaches its equilibrium value of 0°. As the molecule isomerizes around the C_{13}═C_{14} bond and the equilibrium geometry of the 13-cis state is approached, the potential energy on this state decreases (see Figure 2a). In Figure 5a we show the average potential energy, along the nuclear trajectories followed by the initially excited basis functions, on the three relevant electronic states (13-cis, 11-cis, and 15-cis) at five points in time. The arrows in the leftmost panel indicate the overall direction in which the energies move (because of the torsional motion resulting from the optical excitation). The potential energy on the 13-cis state decreases (as the equilibrium value of the torsional coordinate is approached) and it increases on the other two electronic states (because the equilibrium value of the C_{13}═C_{14} torsional coordinate on these states is 180°).

The initial value of the energies combined with the direction in which they move (up or down) explains the time dependence of the non-adiabatic coupling (shown in Figure 4a) and thus of the population transfer (Figure 3a). At early times ($t\rightarrow 0$) the potential energy on the initially excited 13-cis state and on the 11-cis state is similar whereas on the 15-cis state it is lower. Because the variation in the potential energy on the 13-cis state is in the opposite direction to that on the two other states, we immediately see why the 11-cis state is coupled to the 13-cis state for a shorter time than the 15-cis state. The former two states (11- and 13-cis) begin almost in resonance, i.e., with very similar potential energies and hence a large nonadiabatic coupling, and vary from this point in opposite directions. On the other hand, while the potential energies of the 13-cis and 15-cis states also vary in the opposite direction, they begin at quite different energies. In particular because the 15-cis energy is lower than the 13-cis energy they go into and out of resonance and hence the much longer coupling time. There are thus two interesting questions: (i) Why do the energies of the other excited states go up when the energy of the initially excited state goes down and (ii) what determines their initial value, which together with (i) determines the ensuing nonadiabatic dynamics? In the previous paragraph we explained why the potential energy on the initially excited state decreases as a function of time: the torsion angle of the C_{13}═C_{14} bond decreases from an energetically highly unfavorable value (≈180°) to its equilibrium value on this state (0°). As the magnitude of the angle decreases, the potential energy on the two other electronic states increases because their global minimum is at a 13-trans/15-cis or 13-trans/11-cis geometry. The specific value of the initial energies (leftmost panel in Figure 5a) is determined by the vertical excitation energies which are dominated by the difference in dihedral energies. For example, the initial value of the potential energy on the 15-cis state is determined by the all-trans→15-cis vertical excitation energy. From eq 3.1, and ignoring the thermal deviations of the torsional angles from 180° in the all-trans starting material, this is given by $2k^{15-\mathrm{cis}}_{C_{15}=N}$. Since the C_{15}═N bond is softer than the C═C bonds, this bond has a lower excitation energy and hence the low initial energy on the 15-cis state (leftmost panel in Figure 5a).

When the local excitation is confined to the C_{11}═C_{12} bond, i.e., 11-cis state, the time scale for exciton migration to the 13-cis and 9-cis states is the same, yet the branching ratios differ. There is a clear bias (see Figure 3b) toward the Schiff base of the molecule which persists when the magnitude of the interbond nonadiabatic coupling, i.e., coupling between two excited states, is increased, and when the 15-cis state is decoupled from the other electronic states (not shown). As argued above the time scale for exciton transfer, i.e., nonadiabatic coupling between two excited states, is governed by the change in time of the potential energy on each of the relevant electronic states (or in other words by the time duration of the resonances). This is

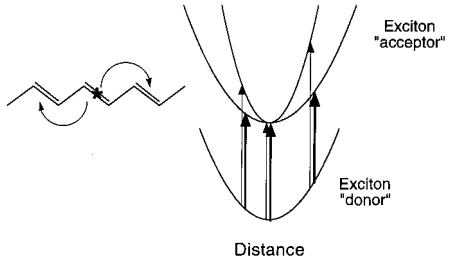

Figure 6. Schematic illustration of the dependence of the energy gap between an initially excited (exciton "donor") state and two other excited (exciton "acceptor") states on the bond stretching frequency. The inset illustrates the initial excitation and the exciton "acceptor" states. Note that since different electronic states correspond to excitation at different bonds, the three harmonic curves are drawn for *different* internuclear bond distances. For clarity the zero of energy of the two "acceptor" states has been shifted upward (in reality the energies of the three states are very close and the "donor" state need not necessarily be below the "acceptor" states). Thick (thin) arrows indicate the energy gap between the "donor" state and an acceptor state with weak (strong) stretching force constant. Other things being equal, as the magnitude of the "acceptor" state force constant decreases so does the energy gap between the "donor" and "acceptor" states.

dominated by the change in torsional angle: the energy decreases on the initially excited state and increases on all the other excited states. In the case of initial excitation of the 11-cis state, the observed time scale is similar because the force constants for the relevant torsions (C_9═C_{10} and C_{13}═C_{14}) are the same. This suggests that in order to explain the bias in branching ratios we must explain a difference in the magnitude of the coupling and not its duration. Furthermore, unlike the discussion of the 13-cis excitation that (correctly) emphasized the role of the torsion force constants, and ignored the smaller effect of the stretches, here we must consider the latter as the former are identical for the relevant states.

The logarithm of the average effective non-adiabatic coupling between the 11-cis state and the 9- and 13-cis states is shown in Figure 4b. In agreement with Figure 3b, the time scale during which the coupling is nonnegligible is similar for both states and the magnitude of the coupling to the 13-cis state is somewhat larger. A larger non-adiabatic coupling implies a "stronger" resonance condition, i.e., a smaller energy gap between the two electronic states. Other things being equal, the absolute magnitude of this gap is determined by the magnitude of the stretching force constant on the 13- and 9-cis states. This result is illustrated in Figure 6. The excitation energy for the different locally excited electronic states is dominated by the torsional energy, which is the same for excitation at any of the C═C bonds. However, its exact value is also determined by the magnitude of the relevant force constant (C═C stretching in this case): as the latter increases, so does the energy gap. On each of the five excited states, the magnitude of the relevant stretching force constant is lower than on the ground all-trans state. The specific values of the stretching force constants (see Table 1) are such that their magnitude increases (by ∼10%) as one recedes from the Schiff base end of RPSB. Thus, the different force constants result in a small energy (and hence resonance) bias that favors the 13-cis state (when compared to the 11-cis state) as shown in Figure 5b. For clarity, the energy scale in parts a and b of Figure 5 is *not* the same and the effect of stretching force constant on the initial value of the potential energy (Figure 5b) is much smaller than that of the torsion (Figure 5a). The direction of the arrows in part b are the same as those in a, for the same reason: the overall direction of change in potential energy is dominated by the dihedral energy which decreases on the 11-cis state and increases on the 13- and 9-cis states. The time scale during which the states are in resonance is therefore similar yet within this given time scale (of ∼100 fs) the energy difference is governed by the magnitude of the different stretching force constants and hence the stronger coupling to the 13-cis state.

Figures 3−6 summarize the main result of this paper: the effect of the interplay between the electronic and nuclear degrees of freedom on exciton transfer and quenching back to the ground electronic state. Quenching and exciton transfer are two temporally disjoint events. The onset of the former requires a substantial motion along the isomerization coordinate and at this point the other excited states are typically decoupled from the initially excited state. Both the time scale for exciton transfer and the specific values of the asymmetric exciton transfer branching ratios are determined by the details of the underlying PESs. We find that within the excited state manifold there is a bias toward low-lying excited states. For RPSB, these states are the ones that involve isomerization around double bonds closer to the Schiff base end. These results are in complete agreement with thermodynamic arguments that invoke electronic energy "funnels." However, we have refrained from invoking any equilibrium assumptions in our explanation, as these would be completely inappropriate for this nonequilibrium problem.

Finally we discuss the expectation values of the nuclear coordinates, in particular the torsions around various double bonds, as a function of time. We remind the reader that the equilibrium configurations on the diabatic PESs are quite different, and that the diabatic electronic states are labeled by these equilibrium configurations. In Figure 7 we plot the expectation values of the C_9═C_{10}, C_{11}═C_{12}, and C_{13}═C_{14} torsion angles (left, middle and right panels, respectively) as a function of time on four electronic states: 9-cis, 11-cis, 13-cis, and all-trans. The initial excitation is localized on the C_{11}═C_{12} bond, i.e., on the 11-cis electronic state. Both the initially excited state (middle panel) and the two exciton photoproduct states (9-cis and 13-cis) photoisomerize on a very similar time scale (≈250 fs). (We note again that although the time scale is similar they photoisomerize around *different* bonds.) On the all-trans electronic state, the three different torsion angles are at a trans configuration (the other two torsions that are not shown are also trans). We have examined the torsion angles (around both single and double bonds) and verified that on each of the five excited states the isomerization is restricted to only one double bond. Furthermore, on the all-trans state all the bonds are in a trans conformation, i.e., thermal photoisomerization is not observed. Therefore, as expected for a large conjugated polyene system, intramolecular energy transfer processes are quite facile and the excitation energy (∼64 kcal/mol) is rapidly redistributed among the various modes so that each of the photoproducts vibrates and librates around its equilibrium position.

IV. Discussion

We have studied the cis−trans photoisomerization of RPSB in order to understand the origin of selectivity in photoproducts. This selectivity has been interpreted in terms of the fundamental competition between excitation migration and quenching by coupling of the electronic and vibrational manifolds. In particular, we have endeavored to understand the limits of the concept of electronic funnels when electron-phonon coupling is strong. Our model of RPSB is characterized by weak nonadiabatic coupling within the manifold of excited electronic states and fast quenching (back) to the ground electronic state.

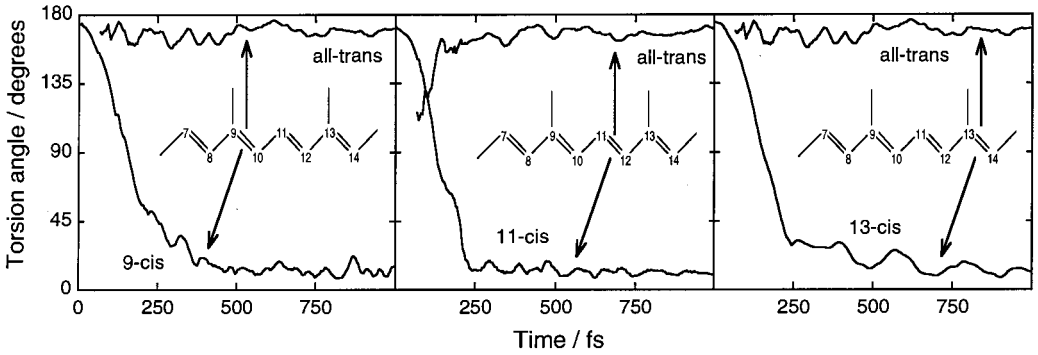

Figure 7. Expectation values of the C_9═C_{10}, C_{11}═C_{12}, and C_{13}═C_{14} dihedral angles (left, middle and right panels, respectively) as a function of time, in femtoseconds, on different electronic states. The initial excitation is to the 11-cis state. The results are averaged over 3 runs and in each run 10 basis functions are used to represent the initial state. Left panel: expectation value of the C_9═C_{10} dihedral angle on the 9-cis state and on the ground all-trans state. Middle panel: the C_{11}═C_{12} dihedral angle on the initially excited 11-cis state and on the ground all-trans state. Right panel: the C_{13}═C_{14} dihedral angle on the 13-cis and all-trans states. Note that the time scale for photoisomerization around different bonds and on different electronic states is similar (≈250 fs).

Thus equilibrium among the various excited diabatic electronic states cannot be achieved before electronic quenching occurs. As pointed out in the introduction, interpreting selectivity in terms of the existence of electronic funnels appears to presuppose that equilibrium in the manifold of electronic excited states is reached before a significant amount of quenching to the electronic ground state occurs. Whether or not the existence of a funnel is relevant in the absence of equilibrium will depend on the relative time scales for exciton migration and electronic quenching, i.e., relaxation among excited electronic states and relaxation between electronic and nuclear degrees of freedom.

Our model of RPSB is constructed to elucidate the consequences of slow equilibration among excited electronic states. Whether this is exactly the case in RPSB is not important for our main point, which is that photoproduct selectivity may be induced by electronic funnels even when equilibrium in the excited state manifold is not reached. The electronic funnel in RPSB arises because of the positive charge on the protonated Schiff base end of the molecule. The ensuing stabilization of ionic character favors electronic excitation near the Schiff base. Our results show that even when electronic excitation migration is slow compared to nuclear rearrangement, this funnel induces a definite preference for migration towards the Schiff base. This is in agreement with the experimental result in hexane,[17] where only three photoproducts are observed: 9-cis (11%), 11-cis (71%), and 13-cis (18%). The analogy with a particle-in-a-box argues that the most favorable excitation will occur in the middle of the conjugated system—in RPSB this is at the C_{11}═C_{12} bond. Thus, it is not surprising that the dominant photoproduct is 11-cis. What is surprising is the preference for 13-cis over 9-cis, and this is explained in our model by the presence of the electronic funnel.

Our interpretation of the role of electronic funnels does not appeal to equilibrium notions at all, but rather emphasizes time-dependent resonances among the electronic excited states. Upon optical excitation, nuclear rearrangement occurs which lowers the potential energy of the optically excited state and raises the potential energy of other excited states. Electronic states that begin at lower energies than the optically excited state, for the initial nuclear geometry, will therefore come into and then go out of resonance with the optically-excited state. On the other hand, electronic states that begin at higher energies will only go out of resonance. Thus, the time scale for non-adiabatic transitions is longer to electronic states that are "down" the electronic funnel, and exciton migration to these states is more efficient. These considerations are expected to be quite general, but a wide range of behaviors may be observed depending on the relative time scales for nuclear rearrangement and excitation migration.

Acknowledgment. We thank Profs. R. D. Levine and P. G. Wolynes for their careful reading of the original manuscript, and Prof. M. A. El-Sayed for lively discussions. This work was partially funded by the NIH (Grant PHS-5-P41-RR05969), NSF (Grant CHE-97-33403), and the UIUC Research Board. M.B.N. thanks the Fulbright and Rothschild Foundations for fellowships. T.J.M. is grateful to the NSF and Research Corporation for support through a CAREER award and Research Innovation Award, respectively.

References and Notes

(1) Bopp, M. A.; Jia, Y.; Li, L.; Cogdell, R. J.; Hochstrasser, R. M. *Proc. Natl. Acad. Sci. USA* **1997**, *94*, 10630.
(2) Vanden Bout, D. A.; Yip, W.-T.; Hu, D.; Fu, D.-K.; Swager, T. M.; Barbara, P. F. *Science* **1997**, *277*, 1074.
(3) Barhaim, A.; Klafter, J.; Kopelman, R. *J. Am. Chem. Soc.* **1997**, *119*, 6197.
(4) Shortreed, M. R.; Swallen, S. F.; Shi, Z. Y.; Tan, W. H.; Xu, Z. F.; Devadoss, C.; Moore, J. S.; Kopelman, R. *J. Phys. Chem.* **1997**, *101B*, 6318.
(5) Ho, W. *J. Phys. Chem.* **1996**, *100*, 13050.
(6) Weinkauf, R.; Schanen, P.; Metsala, A.; Schlag, E. W.; Burgle, M.; Kessler, H. *J. Phys. Chem.* **1996**, *100*, 18567.
(7) Weinkauf, R.; Schlag, E. W.; Martínez, T. J.; Levine, R. D. *J. Phys. Chem.* **1997**, *101A*, 7702.
(8) Remacle, F.; Levine, R. D.; Ratner, M. A. *Chem. Phys. Lett.* **1998**, *285*, 25.
(9) Onuchic, J. N.; Luthey-Schulten, Z.; Wolynes, P. G. *Ann. Rev. Phys. Chem.* **1997**, *48*, 545.
(10) Klessinger, M.; Michl, J. *Excited States and Photochemistry of Organic Molecules*; VCH Publishers: New York, 1995.
(11) Allison, T. C.; Mielke, S. L.; Schwenke, D. W.; Truhlar, D. G. *J. Chem. Soc., Faraday Trans.* **1997**, *93*, 825.
(12) Mathies, R. A.; Lin, S. W.; Ames, J. B.; Pollard, W. T. *Ann. Rev. Biophys. Biophys. Chem.* **1991**, *20*, 491.
(13) Schoenlein, R. W.; Peteanu, L. A.; Mathies, R. A.; Shank, C. V. *Science* **1991**, *254*, 412.
(14) Lanyi, J. K. *J. Bioenerg. Biomembr.* **1992**, *24*, 169−179.
(15) Kochendorfer, G. G.; Mathies, R. A. *Isr. J. Chem.* **1995**, *35*, 211.
(16) Gai, F.; Hasson, K. C.; McDonald, J. C.; Anfinrud, P. A. *Science* **1998**, *279*, 1886−91.
(17) Freedman, K. A.; Becker, R. S. *J. Am. Chem. Soc.* **1986**, *108*, 1245.
(18) Huppert, D.; Rentzepis, P. M. *J. Phys. Chem.* **1986**, *90*, 2813.
(19) Koyama, Y.; Kubo, K.; Komori, M.; Yasuda, H.; Mukai, Y. *J. Photochem. Photobiol.* **1991**, *54*, 433.
(20) Kandori, H.; Sasabe, H. *Chem. Phys. Lett.* **1993**, *216*, 126.
(21) Logunov, S. L.; Song, L.; El-Sayed, M. A. *J. Phys. Chem.* **1996**, *100*, 18586.
(22) Martínez, T. J.; Ben-Nun, M.; Ashkenazi, G. *J. Chem. Phys.* **1996**, *104*, 2847.

(23) Martínez, T. J.; Ben-Nun, M.; Levine, R. D. *J. Phys. Chem.* **1996**, *100*, 7884.
(24) Martínez, T. J.; Ben-Nun, M.; Levine, R. D. *J. Phys. Chem.* **1997**, *101A*, 6389.
(25) Ben-Nun, M.; Martínez, T. J. *J. Chem. Phys.* **1998**, *108*, 7244.
(26) Ben-Nun, M.; Molnar, F.; Lu, H.; Phillips, J. C.; Martínez, T. J.; Schulten, K. *Faraday Disc.* **1998**, *110*. In press.
(27) Heller, E. J. *J. Chem. Phys.* **1975**, *62*, 1544.
(28) Heller, E. J. *Acc. Chem. Res.* **1981**, *14*, 368.
(29) Frenkel, J. *Wave Mechanics: Advanced General Theory*; Clarendon Press: Oxford, 1934.
(30) McLachlan, A. D. *Mol. Phys.* **1964**, *7*, 39.
(31) Kramer, P.; Saraceno, M. *Lecture Notes in Physics, Vol. 140, Geometry of the Time-Dependent Variational Principle*; Springer: Berlin, 1981.
(32) Yarkony, D. R. *J. Phys. Chem.* **1996**, *100*, 18612.
(33) Herman, M. F. *J. Chem. Phys.* **1984**, *81*, 754−763.
(34) Tully, J. C.; Preston, R. K. *J. Chem. Phys.* **1971**, *55*, 562.
(35) Press, W. H.; Teukolsky, S. A.; Vetterling, W. T.; Flannery, B. P. *Numerical Recipes in FORTRAN*; Cambridge Press: Cambridge, 1992.
(36) Santarsiero, B. D.; James, M. N. G.; Mahendran, M.; Childs, R. F. *J. Am. Chem. Soc.* **1990**, *112*, 9416.
(37) Humphrey, W.; Xu, D.; Sheves, M.; Schulten, K. *J. Phys. Chem.* **1995**, *99*, 14549.
(38) Humphrey, W.; Lu, H.; Logunov, I.; Herman, J.; Werner, J.; Schulten, K. *Biophys. J.* **1998**. In press.
(39) Brooks, B. R.; Bruccoleri, R. E.; Olafson, B. D.; States, D. J.; Swaminathan, S.; Karplus, M. *J. Comp. Chem.* **1983**, *4*, 187.
(40) Garavelli, M.; Celani, P.; Bernardi, F.; Robb, M. A.; Olivucci, M. *J. Am. Chem. Soc.* **1997**, *119*, 6891.
(41) Pauling, L. *The Nature of the Chemical Bond*, 3rd ed.; Cornell University Press: Ithaca, 1960.
(42) Herzberg, G. *Molecular Spectra and Molecular Structure, Vol. II, Infrared and Raman Spectra of Polyatomic Molecules*; Krieger: Malabar, FL, 1989.
(43) Ben-Nun, M.; Martínez, T. J.; Levine, R. D. *Chem. Phys. Lett.* **1997**, *270*, 319−326.
(44) Martínez, T. J.; Levine, R. D. *J. Chem. Soc., Faraday Trans.* **1997**, *93*, 940.